Drag Analysis of Hydrokinetic-Savonius Rotor

Anurag Kumar[a], Aditya Veer Gautam[b], Sachendra[c]

[a,b] Mechanical Engineering Department, Rama University, Kanpur, UP. India
[c] Mechanical Engineering Department, KEC, Ghaziabad, UP. India

Abstract- **Small hydropower from the flow streams are populated in research since the construction of large hydro has been in less number and their approval from the ministries in India have become a tedious job for the investors and manufacturers. Hydrokinetic is one of the best options for small hydro development in India. Thus, for design considerations, it is important to find the drag and lift forces for any hydrokinetic turbines (HKT) which design has been modified or newly invented. Drag force is an important parameter for performance and structural stability of HKT turbine. In this research article, a 4-Bladed HKT turbine is analyzed. A complete study of drag and lift forces over the different velocity of flow investigated. Present investigation and calculation are done by the Flow Simulation by Dassault System solver and results are validated by previous experimental investigations.**

Keywords: ***Hydrokinetic, CFD, Fluid, Drag Force, Renewable Energy***

I. INTRODUCTION

The drag coefficient for turbines is more important as its power coefficient. In past drag coefficient has been identified in previous research. However, there is a lack of research available for investigating the hydrokinetic drag forces over water force and pressure enactment. To overcome the issue of energy, need in rural and remote areas it is required the innovative ideas to come up from intellect minds, Researchers and innovators. Hydrokinetic is one of the technologies which can harness the power from water more than the wind turbine than with the same size.

The continuous use of fossil fuels has visible an alarming rise in greenhouse gases ordinarily carbon-di-oxide which in flip has brought about the common upward push in worldwide warming.(Ã & Chiari, 2010)The fossil fuels are not simplest polluting the environment but additionally their fee is increasing every day. The present global society as a consequence begins looking at different avenues for energy (Tavaziani, 2016). In this context, the surroundings-friendly renewable strength has drawn tremendous hobby amongst research groups. A uniform form cross flow over isolated cylinder had studied by (Kundu, P. K., Cohen, I. M., and Hu, 2004) (Zdravkovich, 1997). There are various studies are available for drag reduction over a circular cylinder. (Bouak & Lemay, 2001) proposed the value of the drag about 32% less than other authors. A flow over spinning circular cylinder was studied to investigate the lift and drag coefficient. A vortex shedding was observed for 'a' (ratio of the surface speed and free-stream speed) < 1.91. For a higher rotation rate of the flow, the vortex region takes place only one side.(Mittal & Kumar, 2003). A comprehensive guide is available for fluid flow over different shapes and bodies. This literature accumulates the various experimental studies for flow past over bodies. (Vajravelu & Mukhopadhyay, 2016). A mathematical approach was studied to prevent the cavitations phenomena for underwater hydrokinetics turbine such as marine hydrokinetics. Their proposed methodology modifies the local relative velocity to attain preventive action over cavitations. (Silva et al., 2015)

A simpler based estimation such as Rodriguez and Saturday's (Rodriguez & Sturdza, 2006)(RAGE) rapid geometry engine were used to calculate the drag and lift forces for super ellipse sections. Figure 1 presents four different super ellipses having aU, aL, bU, and bL= 1:0 and using various powers mU=mL = nU= nL. For mU= mL _ nU= nL= 0 the super ellipse is a circle, mU= mL =nU= nL=1:0 makes it a diamond shape, mU= mL = nU= nL<=1:0 demonstrates a chine shape, and mU= mL = nU= nL→∞ leads to a square-shaped section. These examples exhibit the versatility of using super ellipse curves. This parametric geometry enables a conventional (Gur, Mason, & Schetz, 2010) For a two dimensional plane, Y-Z, the coordinates y and z of the super ellipse are defined using the following

relation: where _yc; zc_ is the origin coordinates; a U and a Lare the horizontal half-axis lengths of theupper and lower parts, respectively; band bLare the vertical half-axis lengths of the upper and lower parts, respectively; andmU,mL:nU, and nLare the super ellipse powers that control the cross-sectional shape.

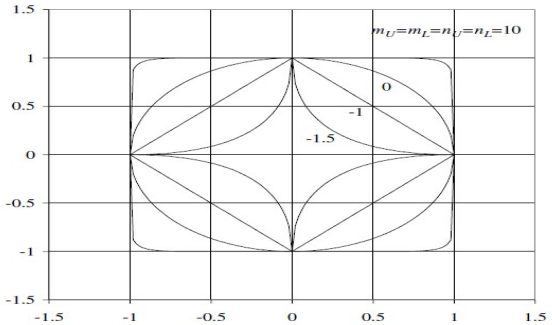

Figure 1: Super ellipse sections used for fuselage-type shapes; aU,aL, bU, and bL=1:0.

Electricity production in line with the turbine properly above that of the first turbine set up and feature generators which may exceed the Betz restriction. Surprisingly farms in tidal straits have proportionately higher blending losses at the back of the generators; consequently, the benefits aren't because of a better turbine conversion performance because the blockage ratio will increase. There is a most excellent range of rows for a farm, but, a harsh diminishing goes back on new rows near this most advantageous will bring about farms being notably smaller than the most fulfilling length. Energy losses due to drag on turbine support shape may be large in multi-row farms, altering their overall performance and limiting farm length. (Vennell, 2012). The 2D computational model is first carried out to research the overall performance of a drag kind rotor design to validate the model via evaluation with experimental measurements. The model added an acceptable accuracy compared to the experimental measurements. The performance of the new design is then investigated using the identical version. The outcomes indicated that the brand new design performance has better electricity coefficient in comparison with unmarried rotor layout. The top energy coefficient of the three rotor turbine is 44% better than that of the single rotor design (relative boom). The stepped forward performance is attributed to the favourable interplay between the rotors which hastens the flow approaching the downstream rotors and generates higher turning moment inside the course of rotation of each rotor.(El-Baz, Youssef, & Mohamed, 2015)

Above reference has been found the lack of drag studies over hydrokinetic turbine has been less studied over the past decades. Thus it important to find the drag coefficient behaviour over different speed and Reynolds number for the four-bladed hydrokinetic turbines. In the present study,a four-bladed semicircular profile of hydrokinetic turbine is kept under the water at nearest to the surface but submerged condition. The turbine is vertical, placed over the water to find out the drag force behaviour and calculations.

A different velocityof the channel stream has taken for the range of 0.5 to 2 m/s. Generally, the velocity of the river stream comes in this range. Above the 2.0 the velocity of a small stream at the summer season can be attain hove ever the turbulence in the stream is more compare to the winter season. It has been investigated the flow behaviour over the 4-Bladed semicircular simonies rotor through the computational model. RANS model has been used to find the critical parameters over the different velocity range..

II. DRAG FORCE OF BLUFF BODIES.

Around-go with the flow styles of bluff bodies under either steady or turbulent ongoing flows had been formed through both 1 shear layer or 2 shear layers on one side or both sides of our bodies due to the drift-body interactions. Depending on characteristics of bluff bodies (sectional form and size) and traits of ongoing go with the flow (consistent or unsteady, wind speed, attack angle) and even in-flow motion of the frame, the round-body waft shear layer can be both balance or instability.

The flow-body interaction phenomena consist of: separation bubble, non-reattachment and reattachment flow, vortex-shedding (1 shear layer or 2 shear layers).

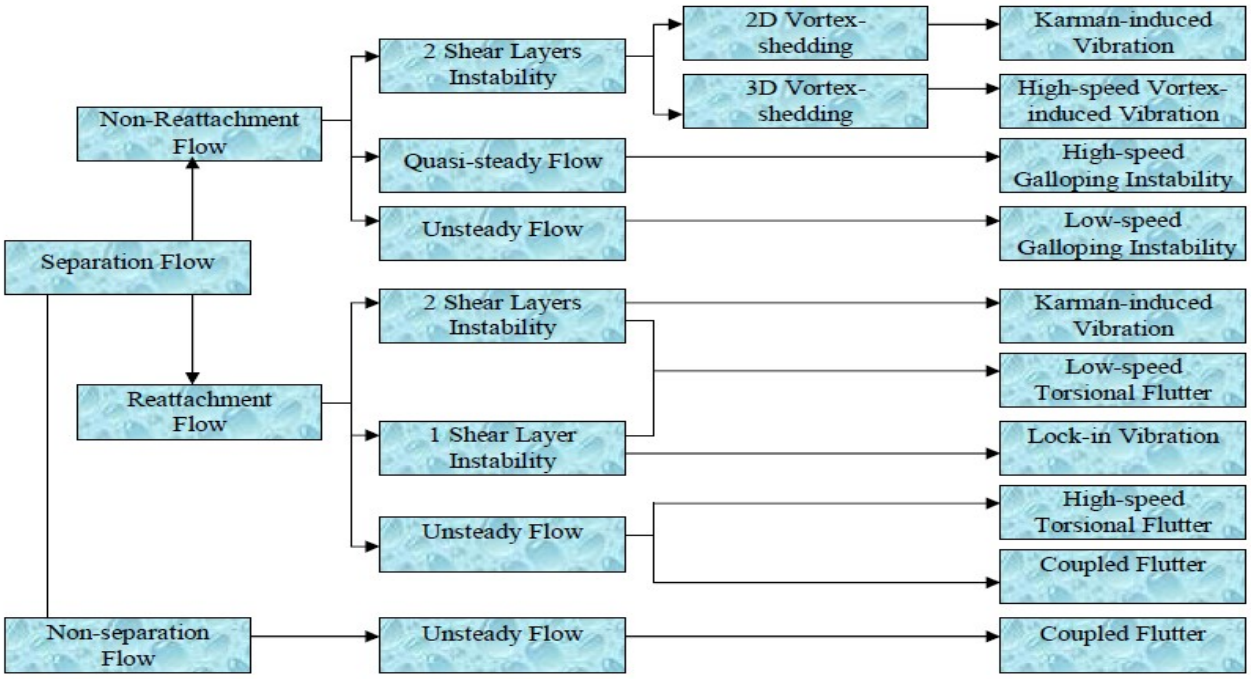

Figure 1: Wind-induced vibrations of Bluff-body aerodynamics(Matsumoto, 1996)

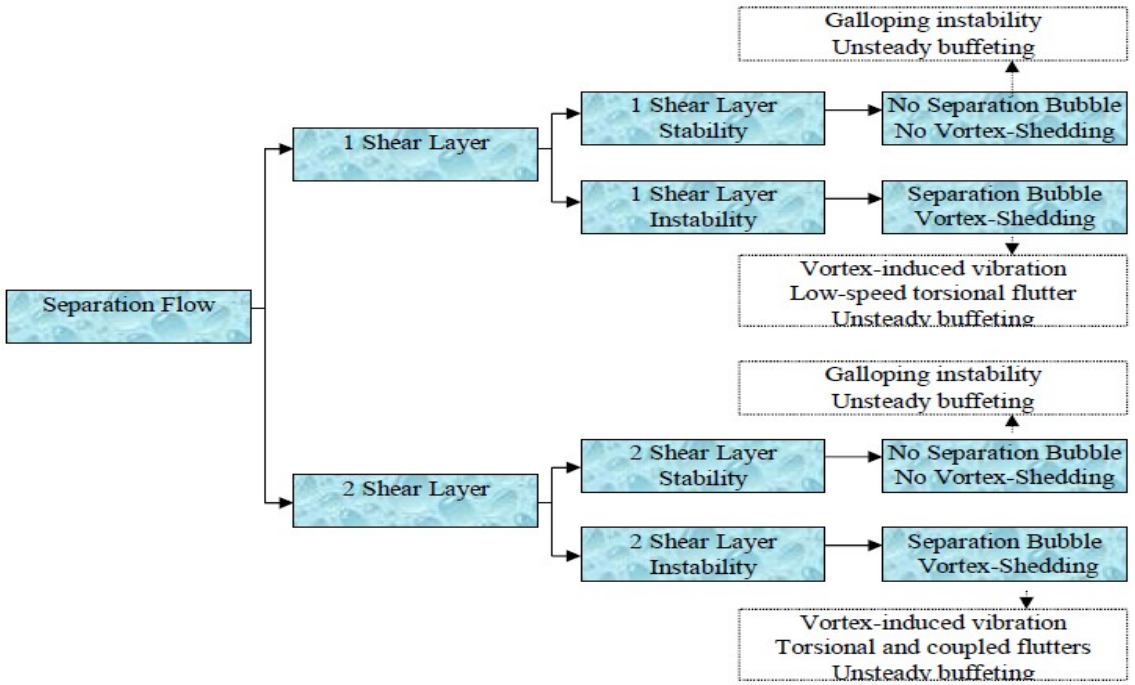

Figure 2: Branches of the shear layer on around-body flow(Matsumoto, 1996)

III. SAVONIUS TURBINE

Generally, hydrokinetics turbine is drag and lift based turbines. For the low-velocity drag based turbines has better starting performance in channels. Its blades are shaped in various manners such as elliptical, semicircular and bend and bend types etc. researchers have been designed and innovate the various models of the blade to improve the performance of rotor. Some of the models are shown in

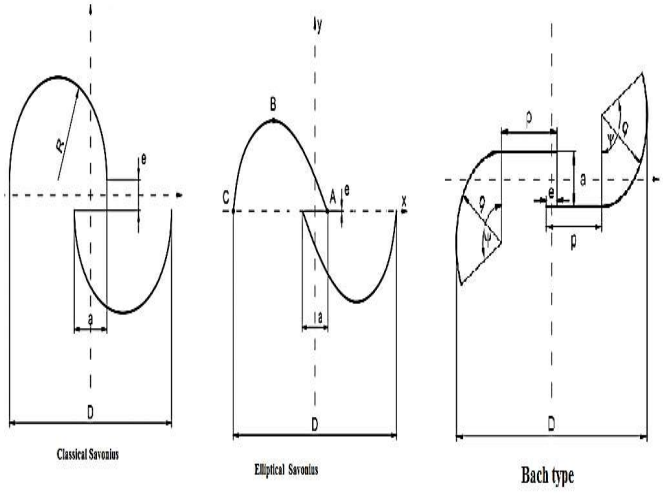

Figure 3: Schematic of Rotors (Kacprzak, Liskiewicz, & Sobczak, 2013)

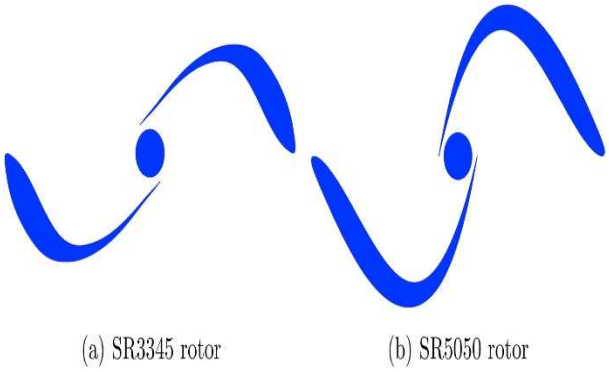

Figure 5: Rotor geometries investigated by (Tartuferi, D'Alessandro, Montelpare, & Ricci, 2015)

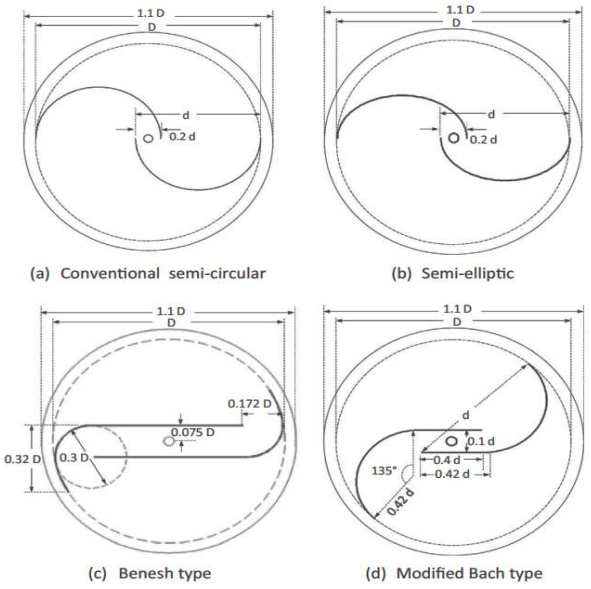

Figure 6: Different profiles of blade investigated by (Roy & Saha, 2015)

Based on the investigations, the optimal geometrical parameters for the modified Savona's hydrokinetic turbine were found to be a twist angle of 12.5°, blade arc angle of 150° and a blade shape factor of 0.6. It has also been found that the coefficient of power increases with the flow velocity. The effect of no. of stages on the performance of this modified turbine was also investigated and a two-stage rotor was found to be optimal. It has been observed that researchers investigated various blade geometry designs to find out the performance over wind or water turbines. Figure 4 explains classical, elliptical and bach type profile. The study concluded that the Bach-type rotor is found to be superior to the other examined geometries in terms of the power coefficient. Figure 5 shows banish conventional semi-elliptic, semi-elliptic and modified Bach types Savona's profile in which modified Savona's profiles gives the best performance over a range of Reynolds number.

Three types of tandem blade Savoniusoverlap, symmetrically and convergence are investigated for hydrokinetic power generation.

IV. DESIGN

A four-bladed (Straight) Semicircular turbine with 1.20 m diameter has been taken for study. **Error! Reference source not found.** shows a schematic of the four-bladed hydrokinetic turbine. The centre shaft diameter of 0.03 m is adopted. Zero overlaps have been chosen for the design for the simplicity of manufacturing. Height of the turbine is considered as 1.43mt. the H/D ration of the turbine is 1.19. This cad model is created on solid works 17.0 version. The thickness of the blade is taken 1.0 mm. 4-bladed are arranged in the equal radial distance by 90 ° apart from each other.

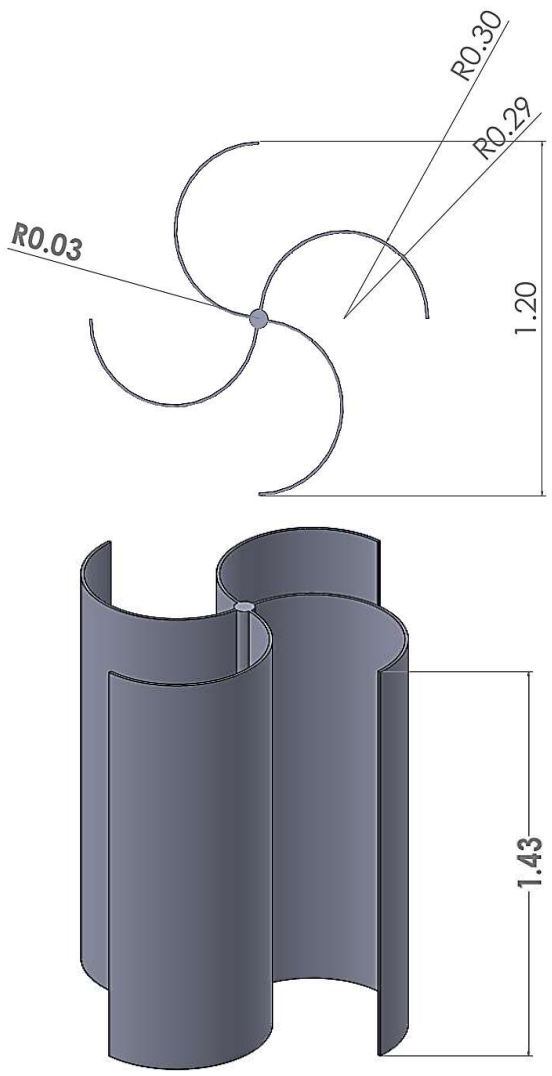

Figure 8: 4 bladed hydrokinetic savonius turbine (a) Tip View (b) Isometric view

V. COMPUTATION & SIMULATION

Computation has been carried out based on the RANS equation for fluid mechanics.

5.1 Boundary Layer Treatment

The alternative approach is to use an immersed-body mesh as shown in Fig. 4. In this approach, the creation of the mesh starts independently from geometry itself and the cells can arbitrarily intersect the boundary between solid and fluid. This makes it possible to use a Cartesian-based mesh, which in the general case cannot be body-fitted. Such a mesh can be defined as a set of cuboids (rectangular cells), which are adjacent to each other and the external boundary of the computational domain, orientated along with the Cartesian coordinates. Mesh generation is started by dividing the rectangular computational domain into a set of rectangular cells (cuboids) formed by the intersection of planes parallel to the axes of the coordinate system. The mesh can be refined (by splitting each cuboid into 8 geometrically-similar cuboids) using various adaptation criteria that can be defined for each solid body (curvature, narrow channels, small features, etc.) and automatically according to gradients in the solution.

5.2 Physical Models

Using one computation mesh having fluid cells, solid cells and (multi-CV) partial cells:
• Fluid flow analysis for fluid regions;
• Heat transfer and direct electrical current calculation in solid regions.
Fluid flow analysis and thermal conduction can also be treated separately. Besides, all these calculations can be coupled with different radiation models. For all these physical phenomena the native CAD geometry remains the source of initial geometric information.

5.2.1 Fluid regions

The Navier-Stokes equations, which are formulations of mass, momentum and energy conservation laws: These

$$\frac{\partial \rho}{\partial t}+\frac{\partial(\rho u_i)}{\partial x_i}=0 \tag{1}$$

$$\frac{\partial(\rho u_i)}{\partial t}+\frac{\partial}{\partial x_j}(\rho u_i u_j)+\frac{\partial P}{\partial x_i}=\frac{\partial}{\partial x_j}(\tau_{ij}+\tau_{ij}^R)+S_i \tag{2}$$

$$\frac{\partial \rho H}{\partial t}+\frac{\partial \rho u_i H}{\partial x_i}=\frac{\partial}{\partial x_i}\left(u_j(\tau_{ij}+\tau_{ij}^R)+q_i\right)+\frac{\partial p}{\partial t}-\tau_{ij}^R\frac{\partial u_i}{\partial x_j}+\rho\varepsilon+S_i u_i+Q_H \tag{3}$$

$$H=h+\frac{u^2}{2}$$

equations are

Supplemented by fluid state equations defining the nature of the fluid, and by empirical dependencies of fluid density, viscosity
And thermal conductivity on temperature. Inelastic non-Newtonian fluids are considered by introducing a dependency whereby their dynamic viscosity is dependent on flow shear rate and temperature. Flow Simulation employs transport equations for the turbulent kinetic energy and its dissipation rate, using the k-ε model. The modified k-ε turbulence model with damping functions proposed by (Lam & Bremhorst, 1981) describes laminar, turbulent, and transitional flows of homogeneous fluids consisting of the following turbulence conservation laws:

$$\frac{\partial \rho k}{\partial t}+\frac{\partial \rho k u_i}{\partial x_i}=\frac{\partial}{\partial x_i}\left(\left(\mu+\frac{\mu_t}{\sigma_k}\right)\frac{\partial k}{\partial x_i}\right)+\tau_{ij}^R\frac{\partial u_i}{\partial x_j}-\rho\varepsilon+\mu_t P_B,$$

$$\frac{\partial \rho \varepsilon}{\partial t}+\frac{\partial \rho \varepsilon u_i}{\partial x_i}=\frac{\partial}{\partial x_i}\left(\left(\mu+\frac{\mu_t}{\sigma_\varepsilon}\right)\frac{\partial \varepsilon}{\partial x_i}\right)+C_{\varepsilon 1}\frac{\varepsilon}{k}\left(f_1\tau_{ij}^R\frac{\partial u_i}{\partial x_j}+C_B\mu_t P_B\right)-f_2 C_{\varepsilon 2}\frac{\rho\varepsilon^2}{k}$$

$$\tau_{ij}=\mu\, s_{ij},\ \tau_{ij}^R=\mu_t\, s_{ij}-\frac{2}{3}\rho k\delta_{ij}\ ,s_{ij}=\frac{\partial u_i}{\partial x_j}+\frac{\partial u_j}{\partial x_i}-\frac{2}{3}\delta_{ij}\frac{\partial u_k}{\partial x_k},$$

$$P_B=-\frac{g_i}{\sigma_B}\frac{1}{\rho}\frac{\partial \rho}{\partial x_i},$$

Where *Cμ=0.09, Cε1 = 1.44, Cε2 =1.92, σk =1, σε=1.3, σB=0.9, CB =1 if PB >0, CB =0 if PB <0,* the turbulent viscosity is determined from:

$$\mu_t=f_\mu\cdot\frac{C_\mu\rho k^2}{\varepsilon},$$

Lam and Bremhorst's damping function fμis determined from:

$$f_1=1+\left(\frac{0.05}{f_\mu}\right)^3,\quad f_2=1-e^{R_t^2}.$$

Lam and Bremhost's damping functions ***fμ, f1, f2*** decrease turbulent viscosity and turbulence energy and increase the turbulence dissipation rate when the Reynolds number *Re* based on the average velocity of fluctuations and distance from the wall becomes too small. When ***fμ****=1, **f1** =1, f2 =1* the approach reverts back to the original ***k-ε*** model.

5.2.2 Fluid Region

Heat transfer in solids and fluids with energy exchange between them (conjugate heat transfer) is an essential and implicit element of CAD-embedded CFD software. Heat transfer in fluids is described by the energy equation (3-4) where the heat flux is defined by (14). The phenomenon of heat conduction in solid media is described by the following equation:

$$\frac{\partial \rho e}{\partial t}=\frac{\partial}{\partial x_i}\left(\lambda_i\frac{\partial T}{\partial x_i}\right)+Q_H$$

Where e is the specific internal energy, e = c•T, c is specific heat, QH is specific heat release (or absorption) rate per unit volume, and λi are the eigen values of the thermal conductivity tensor. It is supposed that the heat conductivity tensor is diagonal in the considered coordinate system. For an isotropic medium λ1 = λ2 = λ3 = λ. In the presence of electric current, QH may include the specific Joule heat release Qj. It is defined as Qj= r•j2, where r is the electrical resistivity and j is the electric current density. The electric current density vector:

$$\mathbf{i}=-\left(\frac{1}{r_{11}}\frac{\partial\varphi}{\partial x_1},\frac{1}{r_{22}}\frac{\partial\varphi}{\partial x_2},\frac{1}{r_{33}}\frac{\partial\varphi}{\partial x_3}\right)$$

Is determined via the electric potential ***φ****[V]* from the steady-state Laplace equation:

$$\frac{\partial}{\partial x_i}\left(\frac{1}{r_{ii}}\frac{\partial\varphi}{\partial x_i}\right)=0$$

Here r***ii*** is the temperature-dependent electrical resistivity in the i-th coordinate direction. The Laplace equation is solved numerically in sub-domains that contain electrically conductive materials. Dielectric solids and fluid areas inside such sub-domains are automatically excluded. The total electric current over a surface I[A] or electric potential φ[V] may be specified by the user as a boundary condition for the problem.

A surface between two electrically-conductive solids in the sub-domain is either considered zero-resistance (the default) or the user can specify an electrical contact resistance on it. The resistance value is either given explicitly or calculated directly from the given material and its thickness. A contact resistance specified on a surface implies that the current passing through it produces the corresponding Joule heating, which gives rise to a surface heat source, as follows.

If the solid consists of several solid materials attached, then the thermal contact resistances between them are taken into account when calculating the heat conduction. As a result, a solid temperature step appears on the contact surfaces. A very thin layer of another material between solids or on a solid in contact with fluid can be taken into account when calculating the heat conduction in solids in the same manner (i.e. as a thermal contact resistance), but is specified via the material's thermal conductivity and the layer thickness.

VI. RESULT DISCUSSION

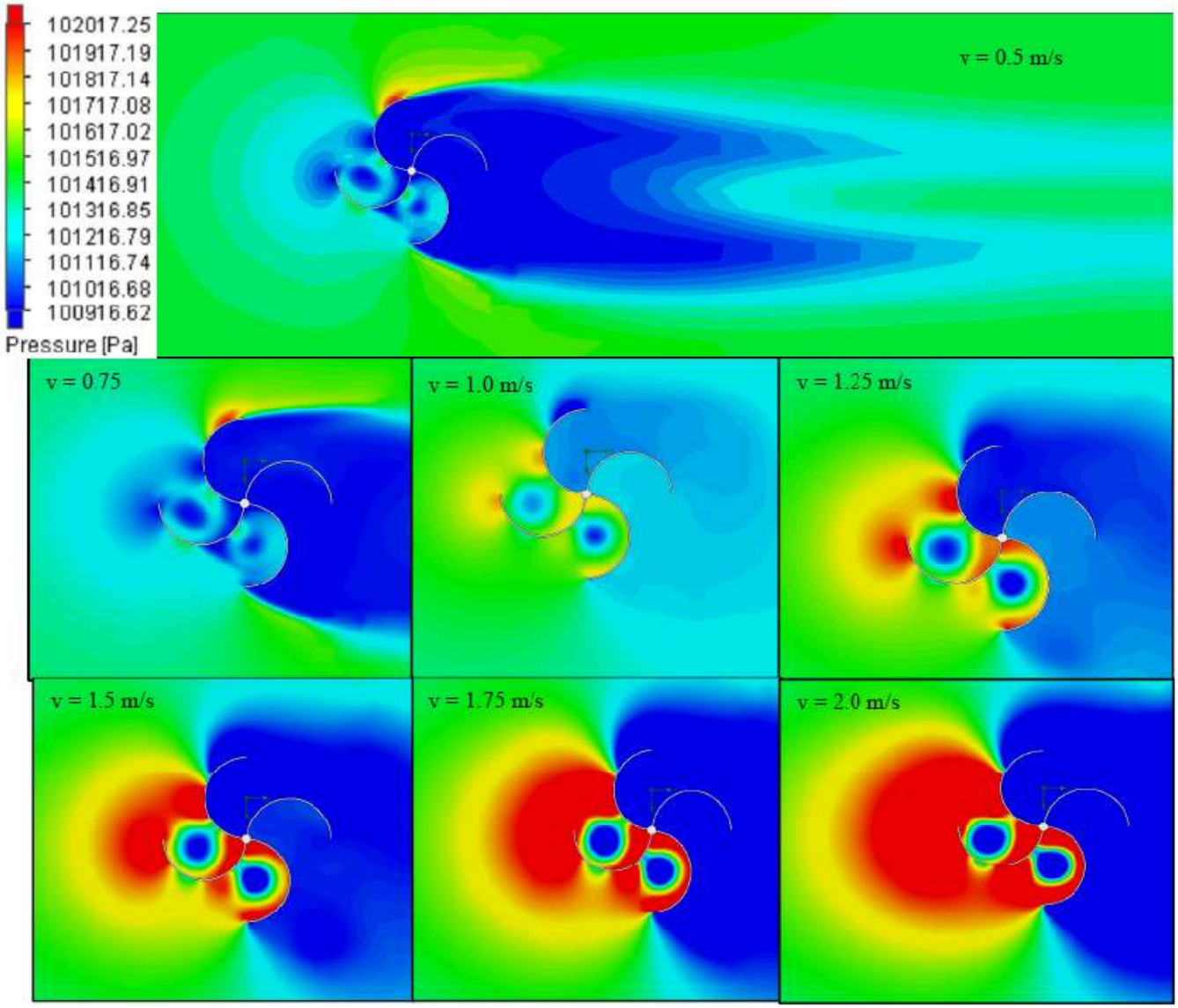

Figure 4: Distribution of pressure contours over the turbine at different inlet velocities of channel

Figure 4 shows the pressure distribution around the savonius rotor. Different velocities contours are shown and pressure variation has recorded for savonius rotor. A transition phase has occurred in the velocities of 1 m/s. It has been seen that the high-pressure zone has been initiated in

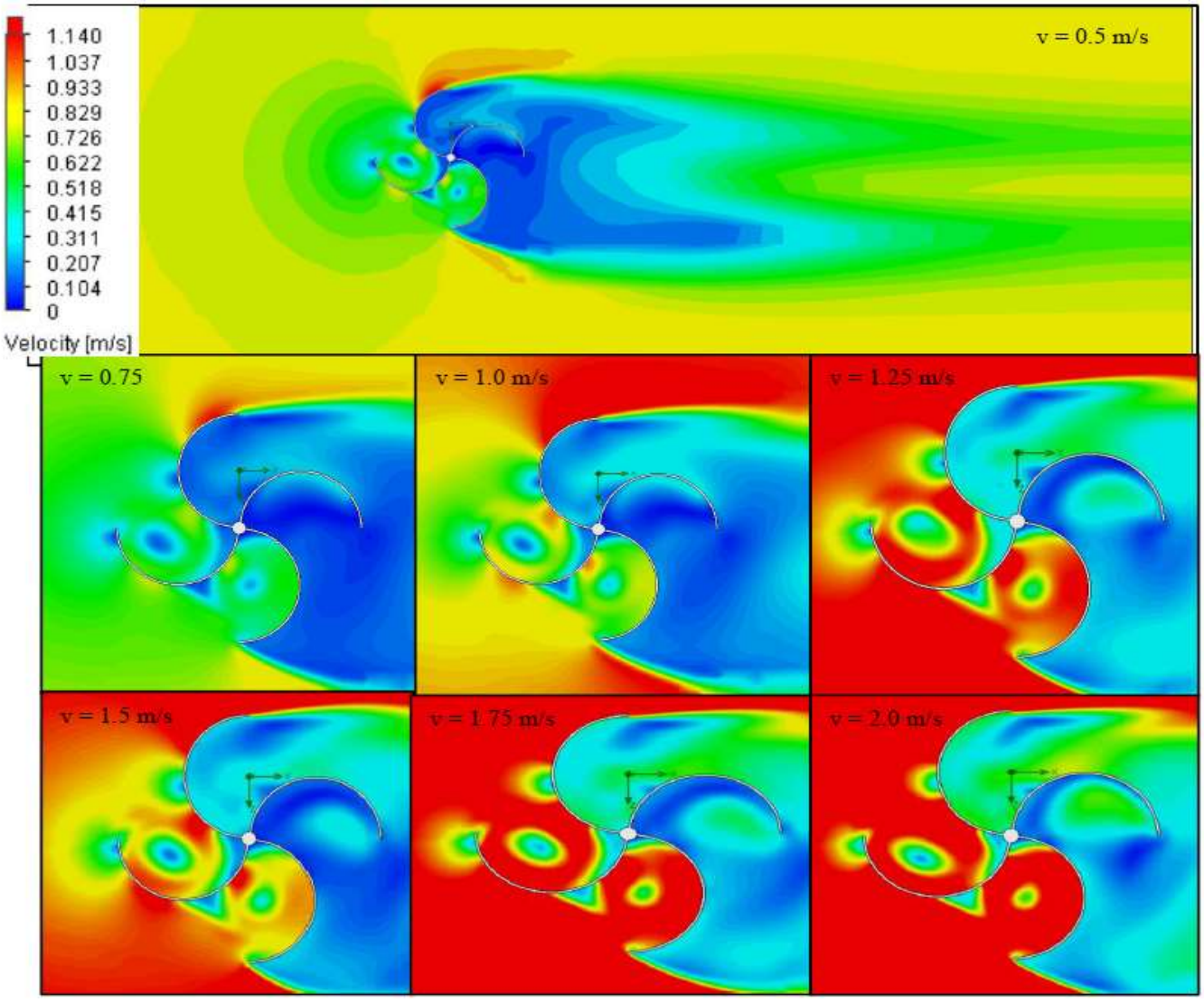

Figure 10: Absolute Velocity contours around the Turbine

Blade 2. At the tip on the velocity of 0.5 m/s. However, it has been changed the location after increase the velocity and it took place at the mid of the blade 2. As velocity increases the high-pressure zone shifted to blade 1 and 4. and a circular zone has emerged for the region of blade 1st and 4th. Behind the blade 2 and 4, the low-pressure zone emerged which creates a rotation force of hydrokinetic turbine.

Figure 10 explains the velocity distribution contours around the savonius rotor, at inlet velocity range of 0.5-2.0 m/s. A high-velocity zone and low-velocity zone can be easily seen on Figure 10, where High velocity or inlet velocity impact to a turbine with its horizontal properties and according to energy equation it velocity get dropped to the lowest value behind the blades such as 1st, 4th, 2nd. Flow separation occurs at the tip of 2nd and 4th number blades. A swirling circle has been created from the starting phase of the velocity and it gets strong as velocity increases.

The week swirl was emerged in 0.5 m/s velocity contour and strong in 2.0 m/s velocity contour. A low-velocity flow separation creates the inclined streamlines towards the wall. However, high-velocity contour has parallel separation lines. The separation of flow is strong in blade 4th rather than blade 2nd at corresponding velocities contours.

Turbulence kinetic energy (TKE) is shown in Figure 11. It is found that TKE for the savonius rotor no exceeds 0.059 J/kg. for all the channel velocities. A turbulence zone has emerged after the midplane of savonius rotor and interior zone of 1st blade. A mild zone of turbulence occurred in the 1st blade region. However, a week turbulence zone can be seen at the tip of the 2nd and 4th blades. Blades tip turbulence created a very large wake region behind the rotor in the flow direction. The zone is strong enough till the 4 -5 meter behind the rotor. It can be observed that turbulence zone length increases as the velocities get an increase.

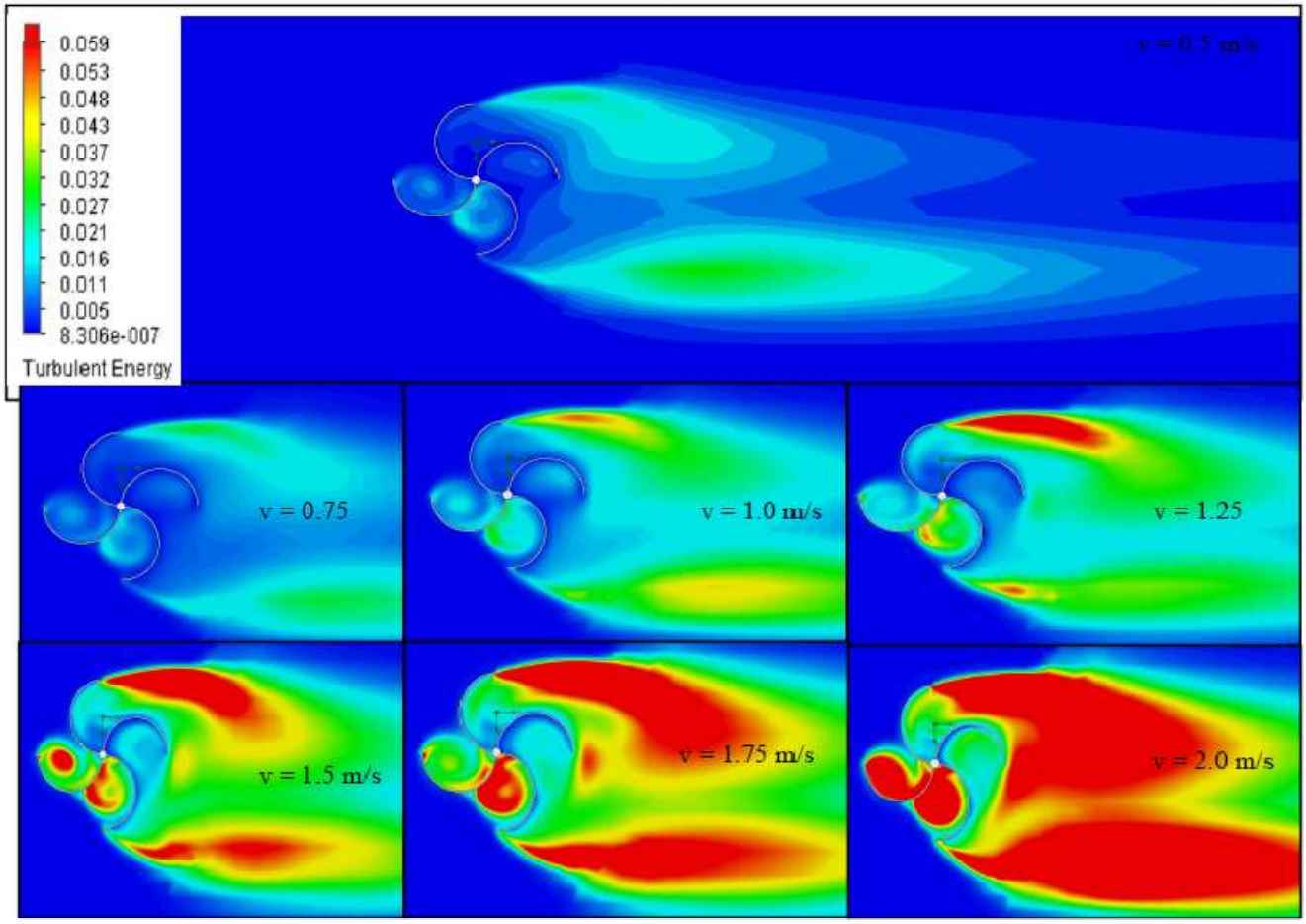

Figure 11. Turbulence Kinetic Energy around the savonius rotor

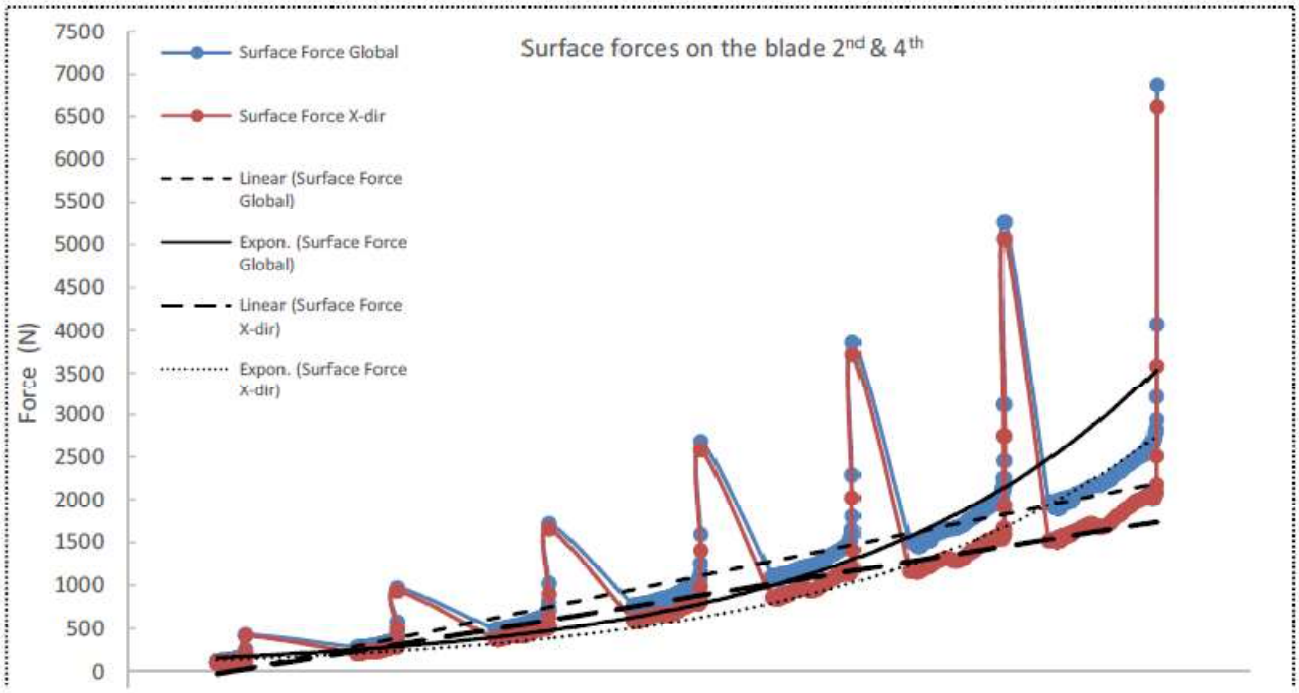

Figure 12 shows, force trends over the different iteration values of velocity and surface forces on the blades. Only those blade surfaces are considered for the calculation which hasa direct impact of the velocity. A trend line is inserted for the best fit curve for both cases such as linear and exponential.

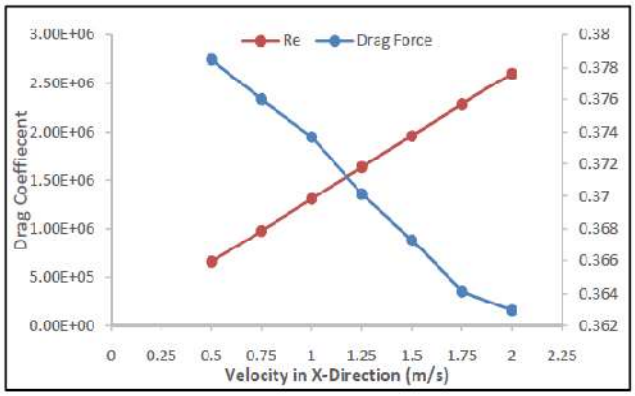

Figure 5: Drag force on the savonius rotor blade

Drag force of the savoinus rotor can be seen through Figure 5. It can be seen that the Reynolds number is Inversely behaving as the drag force decreases. It is the result of the increase in the turbulence created at a higher velocity around the savonius rotor blades. The maximum value of the drag coefficient occurred 0.378 which is typicallynearer as the 0.42 in case of semi-sphere

VII.CONCLUSION

A Hydrokinetic savonius rotor of 4 bladed semicircular has been investigated over the submerged condition of water flow. Different velocities of the water are adopting to flow over the rotor in the range of 0.5 to 2.0 m/s in the 0.5 step size. The rotor is taken as a steady-state condition in a vertical direction and flow of water attack at three blades (1^{st}, 2^{nd} and 3^{rd}). Based on the RANS equation, a drag coefficient and force has been calculated and shown in the contours with the help of Flow Simulation Numerical solver. It has been found the increment of the velocity will decrease the drag coefficient to some extent. This study is done only the velocity range of 2.0 m/s A further study of the different blade profile and velocity will be adopted to an investigated new finding. It has been suggested that there is a lot of scopes to find out the various parameters and the performance of savonius rotor as well as hydrokinetic rotors.

ACKNOWLEDGEMENTS

The authors would like to acknowledge the Rama University, Kanpur and Indian Renewable Energy Development Agency Limited (IREDA) for their support of their research data and reports accesses.

REFERENCES

[1] Ã, A. Z., & Chiari, L. (2010). Fossil-fuel constraints on global warming. Energy Policy, 38(1), 1–3. https://doi.org/10.1016/j.enpol.2009.06.068

[2] Bouak, F., & Lemay, J. (2001). Use of the Wake of a Small Cylinder to Control Unsteady Loads on a Circular Cylinder. Journal of Visualization. https://doi.org/10.1007/BF03182456

[3] El-Baz, A. R., Youssef, K., & Mohamed, M. H. (2015). Innovative improvement of a drag wind turbine performance. Renewable Energy. https://doi.org/10.1016/j.renene.2015.07.102

[4] Gur, O., Mason, W. H., & Schetz, J. A. (2010). Full-configuration drag estimation. Journal of Aircraft. https://doi.org/10.2514/1.47557

[5] Kacprzak, K., Liskiewicz, G., & Sobczak, K. (2013). Numerical investigation of conventional and modified Savonius wind turbines. Renewable Energy. https://doi.org/10.1016/j.renene.2013.06.009

[6] Kundu, P. K., Cohen, I. M., and Hu, H. H. (2004). Fluid mechanics. In Elsevier Academic. Retrieved from https://www.elsevier.com/books/fluid-mechanics/kundu/978-0-12-405935-1

[7] Lam, C. K. G., & Bremhorst, K. (1981). A modified form of the k-ε model for predicting wall turbulence. Journal of Fluids Engineering, Transactions of the ASME. https://doi.org/10.1115/1.3240815

[8] Matsumoto, M. (1996). Aerodynamic damping of prisms. Journal of Wind Engineering and Industrial Aerodynamics. https://doi.org/10.1016/0167-6105(96)00005-0

[9] Mittal, S., & Kumar, B. (2003). Flow past a rotating cylinder. Journal of Fluid Mechanics. https://doi.org/10.1017/S0022112002002938

[10] Rodriguez, D. L., & Sturdza, P. (2006). A rapid geometry engine for preliminary aircraft design. Collection of Technical Papers - 44th AIAA Aerospace Sciences Meeting. https://doi.org/10.2514/6.2006-929

[11] Roy, S., & Saha, U. K. (2015). Wind tunnel experiments of a newly developed two-bladed Savonius-style wind turbine. Applied Energy. https://doi.org/10.1016/j.apenergy.2014.10.022

[12] Silva, P. A. S. F. Da, Shinomiya, L. D., Oliveira, T. F. De, Vaz, J. R. P., Mesquita, A. L. A., & Junior, A. C. P. B. (2015). Design of Hydrokinetic Turbine Blades Considering Cavitation. Energy Procedia. https://doi.org/10.1016/j.egypro.2015.07.343

[13] Tartuferi, M., D'Alessandro, V., Montelpare, S., & Ricci, R. (2015). Enhancement of savonius wind rotor aerodynamic performance: A computational study of new blade shapes and curtain systems. Energy. https://doi.org/10.1016/j.energy.2014.11.023

[14] Tavaziani, A. (2016). Numerical Shape Optimization of a Wind Turbine Blades Using Artificial Bee Colony Algorithm. 137(September 2015), 1–12. https://doi.org/10.1115/1.4031043

[15] Vajravelu, K., & Mukhopadhyay, S. (2016). Flow past a cylinder. In Fluid Flow, Heat and Mass Transfer At Bodies of Different Shapes. https://doi.org/10.1016/b978-0-12-803733-1.00005-3

[16] Vennell, R. (2012). The energetics of large tidal turbine arrays. Renewable Energy. https://doi.org/10.1016/j.renene.2012.04.018

[17] Wahyudi, B., Soeparman, S., Wahyudi, S., & Denny, W. (2013). A Simulation Study of Flow and Pressure

Distribution Patterns in and around of Tandem Blade Rotor of Savonius (TBS) Hydrokinetic Turbine Model. Journal of Clean Energy Technologies, 1(4), 286–291. https://doi.org/10.7763/JOCET.2013.V1.65

[18] Zdravkovich, M. M. (1997). Flowaroundcircular cylinders:Acomprehensive guide through flow phenomena, experiments, applications, mathematical models, and computer simulations. Retrieved from https://trove.nla.gov.au/version/45621824